Proceedings of the ASME 2010 3rd Joint US-European Fluids Engineering Summer Meeting and
8th International Conference on Nanochannels, Microchannels, and Minichannels
FEDSM-ICNMM2010
August 1-5, 2010, Montreal, Canada

FEDSM-ICNMM2010-30213

HEAT FLUX TO FLUIDS WITHIN A ROCK FRACTURE IN A GEOTHERMAL SYSTEM

Dustin Crandall
URS/Washington Division
National Energy Technology Laboratory
Morgantown, WV, USA

Goodarz Ahmadi
Mechanical and Aeronautical Engineering
Clarkson University
Potsdam, NY, USA

Grant Bromhal
National Energy Technology Laboratory
Morgantown, WV, USA

ABSTRACT

Fractures in rocks enable the motion of fluids through the large, hot geologic formations of geothermal reservoirs. The heat transfer from the surrounding rock mass to the fluid flowing through a fracture depends on the geometry of the fracture, the fluid/solid properties, and the flow rate through the fracture. A numerical study was conducted to evaluate the changes in heat transfer to the fluid flowing through a rock fracture with changes in the flow rate. The aperture distribution of the rock fracture, originally created within Berea sandstone and imaged using a CT-scanner, is well described by a Gaussian distribution and has a mean aperture of approximately 0.6 mm. Water was used as the working fluid, enabling an evaluation of the efficiency of heat flux to the fluid along the flow path of a hot dry geothermal system. As the flow through the fracture was increased to a Reynolds number greater than 2300 the effect of channeling through large aperture regions within the fracture were observed to become increasingly important. For the fastest flows modeled the temperature of the working fluids at the outlet of the fracture was reduced due to a shorter residence time of the fluid in the fracture. Understanding what conditions can maximize the amount of energy obtained from fractures within a hot dry geologic field can improve the operation and long-term viability of enhanced geothermal systems.

INTRODUCTION

Enhanced Geothermal Systems (EGS) at Hot Dry Rock (HDR) sites (Duchance and Brown, 2002; Tester et al, 2006) have the potential to become a large source of geothermal power production for the world in the next decades(Lund, Freeston and Boyd, 2005). Since the early 1970s and the Fenton Hill project in New Mexico (Duchance and Brown, 2002) researchers have been attempting to improve the efficiency of geothermal sites by inducing fracture networks within hot rock formations. EGS works by stimulating fractures in otherwise unfractured hot rocks (or in poorly connected fracture networks in hot rocks) and flowing fluids through wells connected to the stimulated fracture networks. In these systems the fracture network conductivity is crucial to ensuring an economic and stable source of energy.

A recent report produced by MIT and the Idaho National Laboratory (Tester et al 2006) identifies areas of improvement that are needed to improve the efficiency of EGS. Of greatest interest to this research is the desire to better understand the influence of major fractures and faults as subsurface conduits to flow and the improved characterization of rock-fluid interactions (Tester et al 2006). Our previous studies have focused on multiphase flows through fractures and the influence of fracture wall roughness on fluid transport (Crandall et al, 2009, 2010). For this study we have modified these previous models to include the effects of heat transfer from hot walls to the initially cooler flowing water. While others have evaluated connectivity of fractured reservoirs (National Research Council, 1997; Selroos et al. 2000), we are choosing to focus on the effects of micro-scale changes on the efficiency of heat transfer from a hot rock to a moving fluid with a fracture. Specifically we evaluate the changes of efficiency with changes in the fluid flow rate changes in the temperature ratio between the initial fluid and the fracture walls. By better characterizing how heat moves to the working fluid within this natural rock fracture geometry we hope to improve predictions of EGS efficiency by identifying parameters in reservoir scale modeling efforts.

NOMENCLATURE

A	Average cross-sectional area of the fracture
b	fracture aperture
c_p	Specific heat
D_h	Hydraulic diameter, 4A/U
E	Total energy
k	Thermal conductivity
L	Fracture length
g	Gravitational acceleration
h	sensible enthalpy
P	Pressure
Q	Volumetric flow rate
Re	Reynolds number, $\rho Q D_h/A_m$
T	Temperature
t	time
U	Perimeter of the average fracture area
u	Fluid velocity
W	Fracture width
Y_j	Mass fraction of species

Greek symbols

κ	Permeability
μ	Dynamic viscosity
θ	Fracture tortuosity
ρ	Fluid density

FRACTURE MODEL GENERATION

The fracture geometry used in this study was created within a 2.5 cm diameter and 9.2 cm long core of Berea sandstone, using a modified Brazilian technique and scanned using computerized tomography (CT) at Penn State University (Karypn et al, 2007). CT scanning of this fracture was performed to determine the fracture properties. The 120 µm voxel (volume pixel) data was 'cleaned' using an in-house code, which removed voids within the rock that were unconnected to the rest of the fracture utilizing VisualLISP and AutoCAD™. The 'cleaned' three-dimensional fracture geometry is shown in Figure 1 along with the length and width of the fracture. In Figure 1 the white regions represent locations of touching fracture walls, zero-aperture locations. The 'as scanned' fracture volume was 1216.37 mm^3 and the cleaned fracture volume was 1214.45 mm^3; a reduction of less than one percent between models.

Apertures within the fracture were measured as the perpendicular distance between the top and bottom fracture walls. Due to the representation as 120 µm voxels in the original data set the measured apertures were binned into 120 µm measurements. The distribution of these apertures is shown in Figure 2. Apertures greater than 1.44 mm comprised less than 0.25% of the data set and are not shown in this distribution. The average aperture for the entire fracture was calculated to be 0.59 mm. As is shown in Figure 2 the fracture is closed along roughly 4% of the area in this model. The percent of closed regions reported by Karpyn et al. (2007) in their original fracture was 1.9%. This indicates that approximately that approximately 2% of the fracture apertures in the scanned fracture were smaller than 120 µm and were not resolved in the 120 µm data set used for this study.

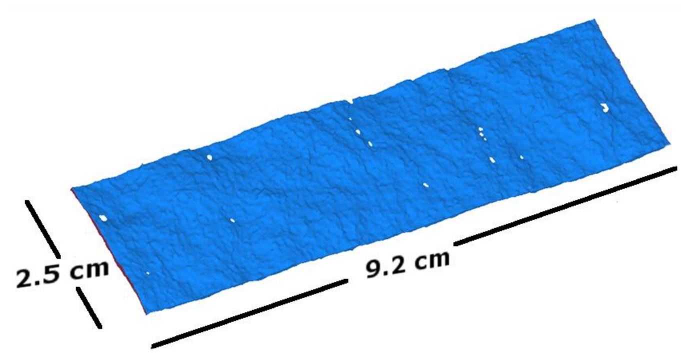

Figure 1: Model fracture geometry.

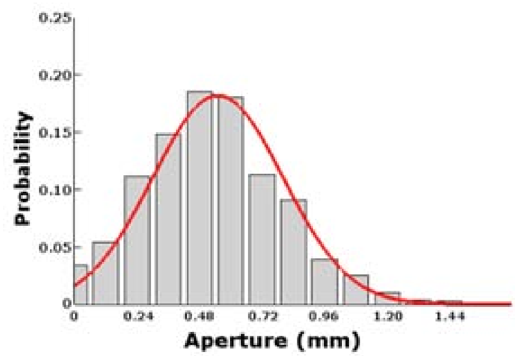

Figure 2: Fracture model aperture distribution.

NUMERICAL MODEL

FLUENT™ was used to solve the steady flow of water through the fracture geometry. The conservation of mass and momentum were solved upon an unstructured, refined mesh of 6 million cells. Conservation of mass is given as,

$$\frac{\partial \rho}{\partial t} + \nabla \cdot (\rho \vec{u}) = 0, \tag{1}$$

and conservation of momentum is given as,

$$\frac{\partial \rho \vec{u}}{\partial t} + \nabla \cdot (\rho \vec{u}\vec{u}) = -\nabla P + \mu \nabla^2 \vec{u} + \rho \vec{g}, \tag{2}$$

where $\vec{g}$ is the acceleration due to gravity, $\vec{u}$ is the fluid velocity, ρ is the water density, t is time, μ is the water viscosity and P is the pressure. In addition the conservation of energy was solved to account for the transfer of energy from the surrounding hot rock walls to the fluid. The conservation of energy for the laminar single fluid flows studied is given as

$$\frac{\partial}{\partial t}(\rho E) + \nabla \cdot (\vec{v}(\rho E + P)) = \nabla \cdot (k \nabla T) \tag{3}$$

where k conductivity, T is the fluid temperature, and E is defined as

$$E = h - \frac{P}{\rho} + \frac{u^2}{2} \tag{4}$$

where h is the sensible enthalpy of the fluid defined as

$$h = \sum_j Y_j h_j \tag{5}$$

where Y_j is the mass fraction of species j and

$$h_j = \int_{T_{ref}}^{T} c_{p,j} dT \tag{6}$$

where $T_{ref} = 298.15\text{K}$.

For the simulations performed water was used as the working fluid with $\rho = 1000\ ^{kg}/_{m^3}$, $c_p = 4182\ ^{J}/_{kgK}$, $k = 0.6\ ^{W}/_{mK}$ and $\mu = 10^{-3}\ ^{kg}/_{ms}$. The solid rough fracture walls were modeled as granite with $\rho = 2750\ ^{kg}/_{m^3}$, $c_p = 790\ ^{J}/_{kgK}$ and $k = 2.5\ ^{W}/_{mK}$.

RESULTS

From the single phase simulations performed the tortuosity, effective permeability, and effective aperture were calculated. These values have been observed to be similar to those expected for flow through a single fracture. The methods used to calculate these properties and the recorded values are discussed here.

Tortuosity, θ, is a quantity that describes the extra distance that a fluid particle will travel as it traverses the macroscopic length of a fracture. This Lagrangian path is longer than the fracture length due to restrictions within the fracture. Thus, θ is a measurement of the heterogeneity of a fracture. To measure this with the numerical model a low injection velocity (0.1 $^{cm}/_{s}$) was applied to a single-phase flow through the fracture and the steady state solution was obtained. Sub-micron particles were released from the constant velocity inlet and the particles were tracked using the step-by-step particle tracker in FLUENT™ (2007). Brownian motion was not included, so that the particles only followed the fluid flow. These step-by-step particle paths were exported as a tab-delineated text file and read into a spreadsheet, with the location of the particle (in Cartesian x, y, and z coordinates) written at time-steps of 10^{-8} s. The distance each particle traveled between each time step, L_i, was calculated from

$$L_i = \sqrt{(x_i - x_{i-1})^2 + (y_i - y_{i-1})^2 + (z_i - z_{i-1})^2} \tag{7}$$

where the subscripts refer to the time steps, i being the current time and $i\text{-}1$ the previous time. L_i was summed over the entire distance the particles traveled and these particle lengths were averaged for all the particles released; ~200 particles were evaluated over the injection face. The θ was calculated with

$$\theta = \frac{\sum L_i}{9.192\,cm} - 1 \tag{8}$$

where 9.192 cm is the macroscopic length of the fracture. The particles were found to travel a distance 9.5% greater than the fracture length, or 10.95 cm. Several representative particle paths are shown in Figure 3.

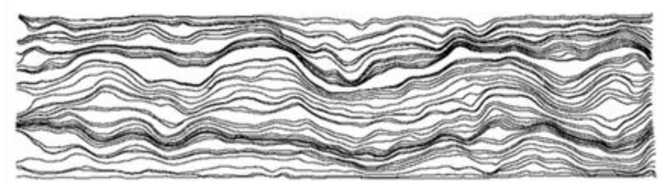

Figure 3: Representative particle pathways through fracture.

Darcy's Law for flow through porous media is often used as an approximation of flow through fracture in reservoir scale simulators (Wu et al. 2004). As shown in Equation 9, Darcy's Law predicts the volumetric flow rate, Q, of a fluid with viscosity μ, for a porous medium with cross-sectional area A, and length perpendicular to the flow L, with an imposed pressure gradient ΔP. The permeability, κ, can be calculated by,

$$\kappa = Q \frac{\mu L}{\Delta P A}. \tag{9}$$

To determine the effective κ of the fracture the full numerical model was run with imposed pressure gradients of 0.1, 1, 10, and 100 Pa across the fracture, and measuring the resultant mass flow rate of water through the fracture. A plot of the recorded flow rates for the case of water as the working fluid is shown in Figure 4.

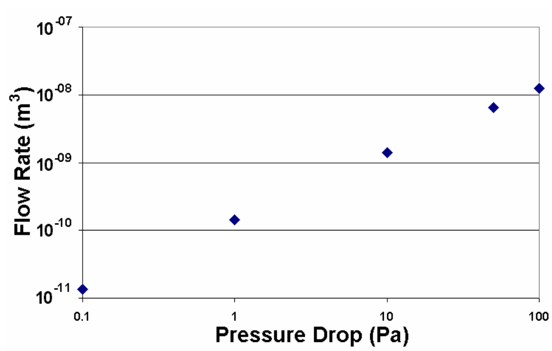

Figure 4: Flow rates of water through full fracture model.

From these results and Equation (9), the effective permeability of the fracture was calculated. Effective permeability refers to the fact that the fracture is not a porous medium, but the narrow aperture resists flow in such a manner that this relationship can be used with some accuracy. The effective permeability was calculated as $1.38(10^{-8})$ m^2 = 14 kD. This is order of magnitudes greater than the κ of the surrounding sandstone (Karypn et al, 2007) and matches well to similar experimental and numerically measured fracture permeabilities.

Using the same ΔP and Q results the effective aperture of the fracture was calculated. The effective aperture assumes that the flow through the fracture can be described by the cubic-law for flow through parallel plates. The cubic law is derived from the Navier-Stokes equations with the assumptions of a narrow aperture, *b*, perpendicular to the flow through a wide and long set of parallel plates (White, 1999). This relation has been used in discrete fracture models and is given as

$$Q = -\frac{b^3 W}{12\mu}\frac{\Delta P}{L} \tag{10}$$

where W is the fracture width and $W >> b$. The effective aperture of the fracture was calculated as 1.1 mm from Equation (10). The similarity of this value to the size of the voxel representation of this fracture indicates that the smallest aperture in the fracture model (1.2 mm) dominates the flow resistance. This has been previously reported in two-dimensional fracture flow studies (Konzuk and Kueper, 2004).

A representative image of velocity vectors through the fracture, with water as the working fluid and with an imposed pressure gradient of 500 Pa is shown in Figure 5. The flow is shown to primarily occur in the narrow constrictions imposed by the heterogeneous geometry in Figure 5. The small, nearly non-existent, flow recorded in regions far from these constrictions is shown in Figure 5 as well. This channeling behavior has been observed in numerical studies (Glass et al. 1998), electrical analogies of flow through fracture (Tsang 1984, Brown et al. 1998), and experimental studies (Karpyn et al. 2009).

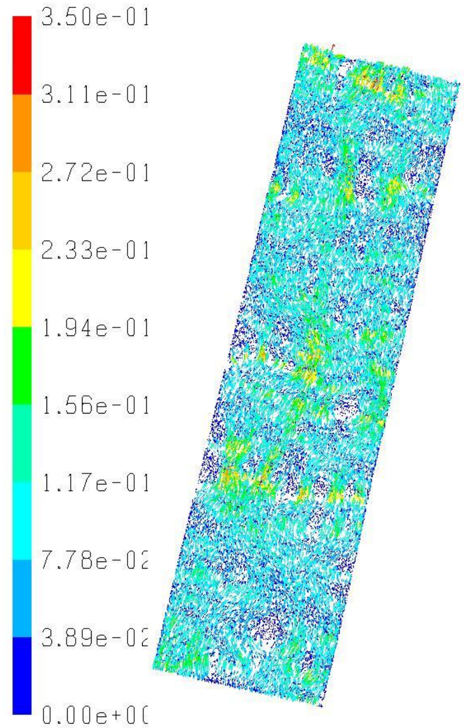

Figure 5: Velocity vectors of water flow due to a 500 Pa pressure gradient through entire fracture. Scale is in $^{m}/_{s}$.

In order to determine the Reynolds Number (*Re*) of flow through the narrow fracture apertures with their rough walls we have used the Re formulation described by Konzuk and Kueper (2002),

$$Re = \frac{\rho Q D_h}{A\mu}, \tag{11}$$

where Q is volumetric flow rate through the fracture, A is the cross-sectional area of the fracture perpendicular to the mean flow and D_h is the mean hydraulic diameter of the fracture, which is defined as

$$D_h = \frac{4A}{U} \tag{12}$$

with U as the perimeter of A.

For this initial study the ρ and μ were assumed constant, the fracture walls were assumed rigid, impermeable and at a constant T and constant P inlet and outlet boundaries were applied. All reported values are the average of the values obtained by flowing water under the same T and ΔP conditions, but in both directions (i.e. the inlet and the outlets were switched and the simulations were repeated). This averaging was done to reduce the influence of directional geometry effects on the reported results. As shown in Figure 6 the resultant distribution of T changed with the direction of the flow. As can be seen in Figure 6 the faster moving flow through the open channels of the fracture tended to heat up only after traveling down a significant portion of the fracture, while slower moving fluid in restricted regions of the fracture warmed to the wall T quickly.

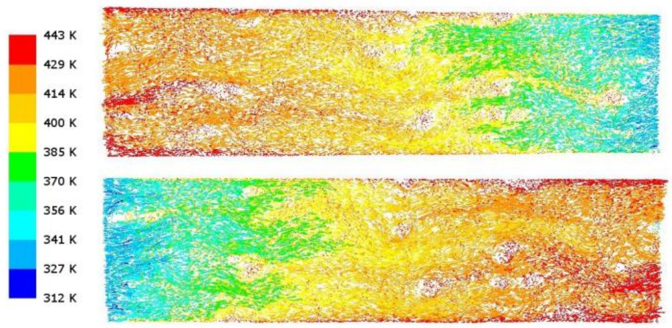

Figure 6: Velocity vectors of water flow under a 2500 Pa ΔP. Colors show T of fluid in Kelvin. Top Image: Flow to the left. Bottom Image: Flow to the right.

The T at the outlet was measured, T_{outlet}. For a suite of simulations with the temperature of the wall, T_{walls}, was set to 440 K (167 °C), the inlet T was set to 330 K (56.8 °C) and ΔP was changed from 50 Pa to 50,000 Pa. The measured ratio of T_{outlet}/T_{walls} is shown for this range in Figure 7. As can be seen the fluid captures most of the energy from the rock walls when the Re < 23000, i.e. T_{outlet}/T_{walls} > 95%. As the velocity is increased the efficiency of the heat transfer decreases and less of the fracture wall energy is picked up by the fluid.

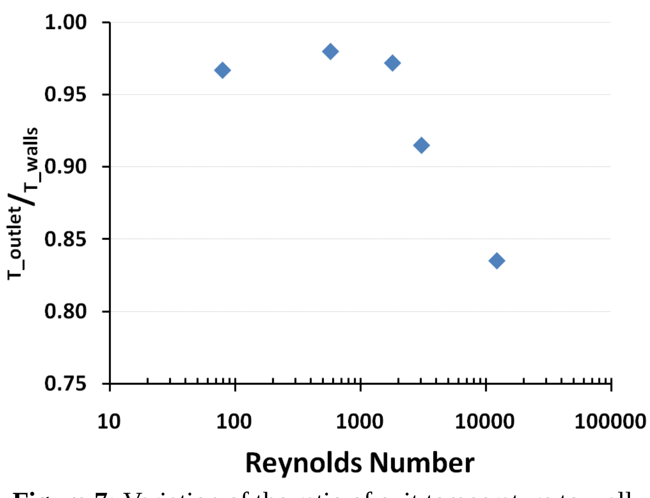

Figure 7: Variation of the ratio of exit temperature to wall temperature with changes in the flow rate.

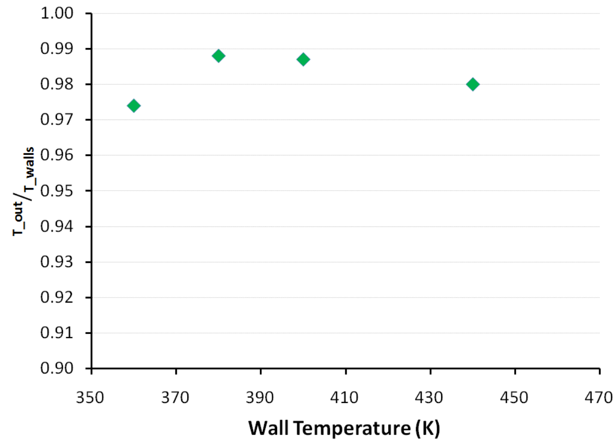

Figure 8: Variation of the ratio of exit temperature to wall temperature with changes in the wall temperature.

For a final set of simulations the T of the surrounding walls were changed and the ΔP was held constant at 500 Pa. As would be expected the ratio of T_{outlet}/T_{walls} did not change significantly with this change in the model parameters, as shown in Figure 8.

CONCLUSIONS

The single phase simulations of water flow through a rough-walled rock fracture described here were shown to capture many of the flow phenomena observed in previous single fracture flow experiments. Namely, the tortuosity and the effective permeability of the fracture were shown to be similar to values described in the literature. Channeling of the working fluid through larger aperture regions of the fracture was observed. This channeling behavior was shown to have an influence on the efficiency with which the higher temperature hot rock walls transferred heat to the water. As the flow rate was increased through the fracture the channeling was observed to become stronger and the efficiency of the working fluid to capture the heat was shown to decline.

Future works building upon this study should evaluate the changes in the heat transfer efficiency with different working fluids, changes to the rock structure with changing temperatures and a decreased heat transfer rate from the rock to the fluids due to mineral deposition. These are physical problems within current EGS fractures and through detailed simulations better parameters describing the pertinent physical processes can be obtained.

ACKNOWLEDGMENTS

This material is declared a work of the U.S. Government and is not subject to copyright protection in the United States. Approved for public release; distribution is unlimited.

REFERENCES

Brown, S. R., Caprihan, A., and Hardy, R. 1998. Experimental Observation of Fluid Flow Channels in a Single Fracture, J. Geophys. Res., 103:5125 – 5132.

Crandall, D., Bromhal, G.S. and Karpyn, Z.T. 2010. Numerical Simulations Examining the Relationship between Wall-Roughness and Fluid Flow in Rock Fractures. Int. J. Rock Mech. Mining Sci. *In Press*.

Crandall, D., Bromhal, G., and Smith, D. H. 2009. Conversion of a Micro-CT Scanned Rock Fracture into a Useful Model. ASME 2009 Fluids Engineering Division Summer Meeting, Paper No. FEDSM2009-78118.

Duchane, D. and Borwn, D. 2002. Hot Dry Rock (HDR) Geothermal Energy Research and Development at Fenton Hill, New Mexico. Geo-Heat Center Quarterly Bulletin, 23(4):13-19.

Karpyn, Z. T., Alajmi, A., Radaelli, F., Halleck, P. M., and Grader, A. S. 2009. X-Ray CT and Hydraulic Evidence for a Relationship between Fracture Conductivity and Adjacent Matrix Porosity, Eng. Geol., 103(3-4):139-145.

Karpyn, Z. T., Grader, A. S., and Halleck, P. M. 2007. Visualization of Fluid Occupancy in a Rough Fracture Using Micro-Tomography, J. Colloid Interface Sci., 307(1):181 – 187.

Konzuk, J. S. and Kueper, B. H. 2004. Evaluation of Cubic Law Based Models Describing Single-Phase Flow Through a Rough-Walled Fracture, Water Resour. Res., 40:W02402

FLUENT 2007. FLUENT 6.3 User's Guide. FLUENT Inc, Lebanon NH.

Glass, R.J., Nicholl, M.J. and Yarrington, L. 1998. A Modified Invasion Percolation Model for Low-Capillary Number Immiscible Displacements in Horizontal Rough Walled Fractures: Influence of Local Inplane Curvature. Water Resour. Res. 34:3215-3234.

Lund, J.W., Freeston, D.H. and Boyd, T.L. 2005. Direct Application of Geothermal Energy: 2005 Worldwide Review. Geothermics34:691-727.

National Research Council, Committee on Fracture Characterization and Fluid Flow. 1996. Rock Fractures and Fluid Flow: Contemporary Understanding and Applications, National Academy Press, Washington D.C.

Selroos, J.-O., Walker, D. D., Ström, A., Gylling, B., and Follin, S. 2002. Comparison of Alternative Modelling Approaches for Groundwater Flow in Fractured Rock. J. Hydrol. 257:174-188.

Tester, J.W. et al. (MIT). 2006. The Future of Geothermal Energy: Impact of Enhanced Geothermal Systems (EGS) on the United States in the 21st Century. Idaho Falls: Idaho National Laboratory. ISBN 0-615-13438-6.

Tsang, Y.W. 1984. The Effect of Tortuosity on Fluid Flow Through a Single Fracture. Water Resour. Res. W0827:1209-1215.

White 1999. Fluid Mechanics, 4th Ed. McGraw Hill: New York NY.

Wu, Y.S, Pan, L. and Pruess, K. 2004. A Physically Based Approach for Modeling Multiphase Fracture-Matrix Interactions in Fractured Porous Media. Adv. Water Res. 27:875-887.